Semiclassical scattering theory based on the dynamical-state representation: Application to the $Li^+ + Na$ and $Li + Na^+$ collisions

Reiko Suzuki*
Division of Theoretical Studies, Institute for Molecular Science, Myodaiji, Okazaki 444, Japan and Department of Physics, Ochanomizu University, Otsuka, Bunkyo-ku, Tokyo 112, Japan

Hiroki Nakamura
Division of Theoretical Studies, Institute for Molecular Science, Myodaiji, Okazaki 444, Japan

Eiichi Ishiguro
Department of Physics, Ochanomizu University, Otsuka, Bunkyo-ku, Tokyo 112, Japan
(Received 28 December 1983)

A purely theoretical semiclassical method without any ambiguity is presented for the calculation of differential cross sections for atomic collision processes involving both radial and rotational (Coriolis) nonadiabatic couplings. The method is based on the recently proposed dynamical-state representation, which enables us to deal with radial and rotational couplings in a unified way. This theory is applied to the asymmetric charge transfer and excitation in the $Li^+ + Na$ and $Li + Na^+$ collisions. The calculated differential cross sections are in good agreement with experimental results.

I. INTRODUCTION

It is well known that atomic collision processes involving lower electronically excited states are governed by nonadiabatic radial and rotational couplings. Nonadiabatic radial coupling is the mechanism which causes a transition between adiabatic electronic states of the same symmetry, and can be dealt with analytically by the semiclassical theories such as the Landau-Zener-Stueckelberg and the Rosen-Zener formula. On the other hand, nonadiabatic rotational (or Coriolis) coupling causes a transition between adiabatic states of different electronic symmetry. Having properties quite different from those of radial coupling, rotational coupling can not straightforwardly be cast into the framework of the conventional semiclassical theories.

The recently proposed dynamical-state (DS) representation[1,2] makes a uniform treatment of radial and rotational couplings possible. Since the rotational coupling is diagonal in this representation, all of the transitions among the DS's are induced by a radial coupling, namely by the operator $\partial/\partial R$ with R being the internuclear distance. In addition, since the analytical properties of the DS representation are the same as those of the radial coupling problem in the adiabatic-state representation, the conventional semiclassical theories can be utilized only with a replacement of the adiabatic-state energies by the DS energies. The underlying basic philosophy of this representation is quite general, and is the same as that of the adiabatic-angular-function representation in electron-molecule collisions[3] and of the adiabatic-state representation in the hyperspherical coordinate approach.[4,5]

Alkali diatomic molecular ions (for example, Na_2^+, $LiNa^+$, LiK^+, and NaK^+) have been good targets of experimental as well as theoretical investigations.[6–16] Since these molecules are quasi-one-electron systems, the adiabatic potential energies can be calculated by the effective potential method. The lowest molecular states (1Σ and 2Σ) are coupled to each other by radial coupling, and the second (2Σ) and the third (1Π) states are rotationally coupled (see Fig. 1). In the case of homonuclear ions (i.e., Na_2^+) the lowest two states represent the so-called exact resonance states which are degenerate at $R=\infty$, and are not coupled *dynamically* to each other. In the case of heteronuclear ions[9(b),10] the distinction between *gerade* and *ungerade* symmetry breaks down and the radial coupling becomes important. This radial coupling is the

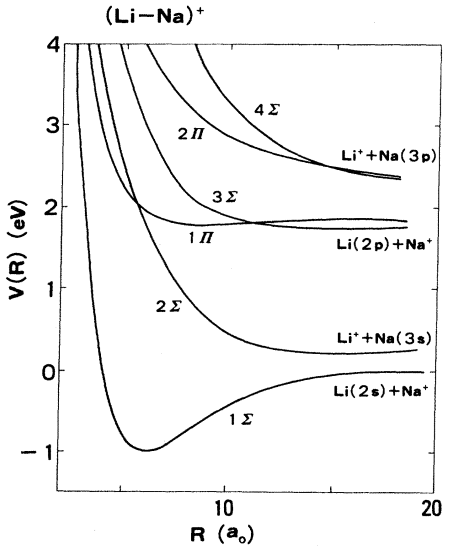

FIG. 1. Adiabatic potential energy curves of $LiNa^+$.

near-resonant type, or the Rosen-Zener type. The coupling becomes, however, unimportant again in the case of strong heterogeneity (i.e., LiK^+ and NaK^+),[9(b)] because the energy difference between 1Σ and 2Σ becomes too large for the transition to occur effectively.

The $(Li\text{-}Na)^+$ system has been a target of a number of experimental and theoretical investigations.[6–8,10–16] Differential cross sections for elastic and inelastic scattering have been measured at energies of 25—135 eV by von Busch *et al.*,[7] of 200—1200 eV by Wijnaendts van Resandt *et al.*,[10] and of 750—2000 eV by Okamoto *et al.*[12] Theoretical calculations of total and differential cross sections have also been carried out by many authors. Total inelastic cross sections were calculated by Melius and Goddard,[6] who solved the time-dependent coupled equations using the straight-line trajectory approximation. They showed that it is adequate to consider only the lowest three (1Σ, 2Σ, and 1Π) states for the study of the processes we are interested in [see Eq. (1.1) below]. They found an undulation of cross sections against collision energy in the case of the 1Σ-2Σ transition. Other authors employed certain kind of semiclassical theories to calculate differential cross sections. From our viewpoint, however, none of them can be free from ambiguity, concerning especially the treatment of rotational coupling. Grosser[11] neglected the effect of rotational coupling on the transition between 1Σ and 2Σ. Wijnaendts van Resandt *et al.*[10] assumed a Gaussian function of impact parameter for the 2Σ-1Π transition probability, neglecting the phase information completely. Okamoto *et al.*[12] employed the similar approximation with the phase contribution included. They assumed, however, a rotationally induced transition to occur exclusively at a turning point. This is not a good approximation in the adiabatic-state representation. Furthermore, in the analysis of the Σ-Σ transition Wijnaendts van Resandt *et al.* employed the crossing "quasidiabatic" potentials. The physical meaning of these potentials is not clear and their treatment is not consistent. As is mentioned above, the semiclassical path-integral formalism based on the DS representation enables us to deal with unambiguously both radial and rotational couplings with the phase information correctly taken into account.

In the present paper this formalism is applied to analyze the processes,

$$\mathrm{Li}(2s)+\mathrm{Na}^+\rightarrow\mathrm{Li}^+ +\mathrm{Na}(3s),\quad \mathrm{Li}(2p)+\mathrm{Na}^+$$

and (1.1)

$$\mathrm{Li}^+ +\mathrm{Na}(3s)\rightarrow\mathrm{Li}(2s)+\mathrm{Na}^+,\quad \mathrm{Li}(2p)+\mathrm{Na}^+ .$$

The adiabatic potential energy curves we have employed are the analytical expressions fitted by Wijnaendts van Resandt *et al.*[10] to the numerical results obtained by Habitz and Schwarz.[8] At small R [$\lesssim(1.6\text{–}2.6)a_0$] we have smoothly extrapolated their curves by using the functions $C_1/R+C_2$, where C_1 and C_2 are constants. The plan of this paper is as follows. In Sec. II the semiclassical theory in the DS representation is presented. Methods for calculating differential as well as total cross sections are described with use of the new representation. The validity of the semiclassical theory for a rotationally induced transition is also demonstrated in this section by taking a two-state (2Σ and 1Π) system. The calculated results on total and differential cross sections for the processes (1.1) are presented in Secs. III and IV. The rotational coupling effect is clearly manifested in the differential cross sections. Agreement of the differential cross sections with experiments seems satisfactory, indicating the usefulness of our semiclassical theory based on the DS representation. The calculated total cross sections for the $1\Sigma\rightarrow2\Sigma$ ($1\Sigma\rightarrow1\Pi$ and $2\Sigma\rightarrow1\Pi$) transition are, however, larger (smaller) than those of Melius and Goddard.[6] This disagreement is attributed to a slight difference of the potential energy curves of Habitz and Schwarz from those of Melius and Goddard at large R ($\gtrsim 12a_0$), since the probability of the Rosen-Zener—type transition is sensitive to the slight variation of the R dependence of the potential energies of the 1Σ and 2Σ states at large R.

II. SEMICLASSICAL SCATTERING THEORY IN THE DYNAMICAL-STATE REPRESENTATION

A. Dynamical-state potential energies

The total Hamiltonian of a diatomic system is given by[2]

$$H=-\frac{\hbar^2}{2\mu R^2}\frac{\partial}{\partial R}R^2\frac{\partial}{\partial R}+H_{\mathrm{rot}}+H_{\mathrm{el}}+H_{\mathrm{Cor}} , \tag{2.1}$$

where μ is the reduced mass of the collision system, H_{rot} represents the rotation of a diatomic molecule, H_{el} represents electronic Hamiltonian, and H_{Cor} denotes the Coriolis interaction given by

$$H_{\mathrm{Cor}}=\frac{\hbar^2}{2\mu R^2}L^2-\frac{\hbar^2}{2\mu R^2}(L_+U_+ +L_-U_-) , \tag{2.2}$$

with

$$L_\pm=L_\xi\pm iL_\eta \tag{2.3}$$

and

$$U_\pm=\mp\frac{\partial}{\partial\theta}+\frac{i}{\sin\theta}\frac{\partial}{\partial\varphi}+L_\zeta\cot\theta . \tag{2.4}$$

The angles θ and φ are the ordinary angle variables to define the molecular axis orientation, L is the electronic orbital angular momentum, and L_ξ, L_η, and L_ζ are components of L in the molecule fixed-coordinate system with the ζ axis along the molecular axis.

Let us define the adiabatic electronic eigenfunctions $\phi_j(\Lambda;\vec{r}:R)$ and corresponding eigenvalues $\epsilon_j(\Lambda:R)$ of H_{el} by

$$H_{\mathrm{el}}\phi_j(\Lambda;\vec{r}:R)=\epsilon_j(\Lambda:R)\phi_j(\Lambda;\vec{r}:R) . \tag{2.5}$$

The dynamical states are defined as the eigenstates of

$$H_{\mathrm{dyn}}\equiv H_{\mathrm{el}}+H_{\mathrm{rot}}+H_{\mathrm{Cor}} \tag{2.6}$$

by

$$H_{\mathrm{dyn}}\Psi_j^K(\vec{r},\hat{R}:R)=E_j^K(R)\psi_j^K(\vec{r},\hat{R}:R) , \tag{2.7}$$

where $\hat{R}=(\theta,\varphi)$, and K is the total angular momentum quantum number. If we introduce the electronic-rotational basis functions by

$$\Phi^K_{\pm j}(\Lambda)=\frac{1}{\sqrt{2}}\{\phi_j(\Lambda^+;\vec{r}:R)Y(K\Lambda^+;\hat{R}) \pm\phi_j(\Lambda^-;\vec{r}:R)Y(K\Lambda^-;\hat{R})\} \text{ for } \Lambda\neq 0 \quad (2.8)$$

and

$$\Phi^K_{\pm j}(\Sigma)=\phi_j(\Sigma^{\pm};\vec{r}:R)Y(K0;\hat{R}) \text{ for } \Lambda=0\,, \quad (2.9)$$

where $Y(K\Lambda;\hat{R})$ is an eigenfuntion of $H_{\rm rot}$,

$$H_{\rm rot}Y(K\Lambda;\hat{R})=[K(K+1)-2\Lambda^2]Y(K\Lambda;\hat{R})\,, \quad (2.10)$$

and $\Lambda^{\pm}=\pm|\Lambda|$, and then the whole set of states $\{\Phi^K_{\pm j}(\Lambda)\}$ can be divided into two classes $\{\Phi^K_{+j}(\Lambda)\}$ and $\{\Phi^K_{-j}(\Lambda)\}$ which have no connection to each other. The DS's are thus expanded in terms of the electronic-rotational states of either class as

$$\Psi^K_j(\vec{r},\hat{R}:R)=\sum_k C^K_{jk}(R)\Phi^K_{+k}(\Lambda) \quad (2.11a)$$

or

$$\Psi^K_j(\vec{r},\hat{R}:R)=\sum_k D^K_{jk}(R)\Phi^K_{-k}(\Lambda)\,. \quad (2.11b)$$

The dynamical-state energies $E^K_j(R)$ can be obtained by diagonalizing the matrix $\{(H_{\rm dyn})_{ij}\}$ in the electronic-rotational state representation. The jth diagonal element of this matrix is given by

$$\epsilon^K_j(R)=\epsilon_j(\Lambda:R)+\frac{\hbar^2}{2\mu R^2}[K(K+1)-2\Lambda^2] +\frac{\hbar^2}{2\mu R^2}\langle L^2\rangle_{\Lambda}\,. \quad (2.12)$$

The Coriolis interaction $H_{\rm Cor}$ provides an off-diagonal element as

$$\langle\Phi^K_{\pm i}(\Lambda_i)|H_{\rm Cor}|\Phi^K_{\pm j}(\Lambda_j)\rangle=-\frac{\hbar^2}{2\mu R^2}\{\lambda_-(K,\Lambda_j^+)\delta(\Lambda_i^+,\Lambda_j^+-1)\langle\phi_i(\Lambda_i^+)|L_-|\phi_j(\Lambda_j^+)\rangle +\lambda_+(K,\Lambda_j^+)\delta(\Lambda_i^+,\Lambda_j^++1)\langle\phi_i(\Lambda_i^+)|L_+|\phi_j(\Lambda_j^+)\rangle\}\,, \quad (2.13)$$

where

$$\lambda_{\pm}(K,\Lambda)=[(K\mp\Lambda)(K\pm\Lambda+1)]^{1/2}\,. \quad (2.14)$$

Thus basic quantities necessary to determine dynamical-state energies are the adiabatic potential energies $\epsilon_j(\Lambda:R)$ and the rotational coupling matrix elements

$$V_{ij}=\langle\phi_i(\Lambda_i^+)|L_-|\phi_j(\Lambda_j^+)\rangle\,. \quad (2.15)$$

Properties of the dynamical states defined above are summarized as follows.[5]

(1) The states are the eigenstates of the rotating collision complex at fixed R, and are thus dependent on the total angular momentum quantum number.

(2) All the coupled states avoid crossing.

(3) All the transitions among them are caused exclusively by the first term of Eq. (2.1).

(4) Analytical properties of the dynamical-state representation are the same as those of the ordinary radial coupling problem in the adiabatic-state representation.

These properties lead us to conclude that all the nonadiabatic transitions occur locally at new avoided crossing points and can be treated uniformly by the semiclassical theories such as the Landau-Zener-Stuckelberg and Rosen-Zener formulas.[17] These properties hold true for any transitions, in principle, in more complicated systems, if we employ the hyperspherical coordinate system (the hyperradius plays the role of R).[5]

The adiabatic potential energies of the low-lying states of $LiNa^+$ were calculated by Habitz and Schwarz[8] by using the effective core-potential method. Analytical functions were fitted to their potential energies.[10] Melius and Goddard also calculated the potential energies.[6] We have employed in our analysis the analytical fits to the energies of Habitz and Schwartz, since we need analytical expressions in our theory. Since the fitting parameters for the 1Π state given in Ref. 10 seem to be in errors, we have used the following values: $(\alpha,A)=(0.1,0.13127)$, $(0.4,-10.541)$, $(0.6,46.181)$, $(0.8,-32.327)$, and $(1.5,87.254)$, where α (in a_0^{-1}) and A (in eV) have the same meaning as those in Ref. 10. The potential curves are shown in Fig. 1. It has been proven[6] that only the lowest three states (1Σ, 2Σ, and 1Π) are sufficient to be considered in order to investigate the processes (1.1) at collision energies below several keV. The transition between 3Σ and 1Π is not required to be taken into account, because we are interested only in the total production of $Li(2p)$. The rotational coupling between 3Σ and 1Π states should, in principle, affect the transition between 1Π and 2Σ states, as was discussed before under the name of catalysis effect.[1(b)] In reality, however, the rotational coupling matrix element between 3Σ and 1Π states happens to be very small in the region of the crossing of 1Π and 2Σ states.[6] Therefore, in the following analysis we consider only the lowest three states. The rotational coupling element $V_{2\Sigma,1\Pi}$ defined by Eq. (2.15) is taken from the calculations by Melius and Goddard[6] (Fig. 2). Their result is analytically fitted by a simple function of R. Another important coupling in this system is the one between 1Σ and 2Σ states at large R. This is a radial coupling of the Rosen-Zener type. The corresponding nonadiabatic radial coupling matrix element is not necessary in our procedure since we perform an analytic continuation of the adiabatic or the dynamical-state potential energies into the complex R plane. Figure 3 shows an example of the dynamical-state potential curves for $K=1700$.

B. Scattering matrix in multistate collision problem

Since in the DS representation nonadiabatic transitions occur locally at new avoided crossing points, a multistate

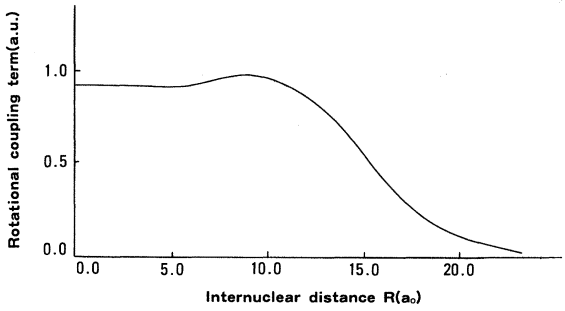

FIG. 2. Rotational coupling matrix element between 2Σ and 1Π states.

scattering problem can be formulated analytically by using the two-state semiclassical theories and the path-integral formalism. In the present three-state problem (Fig. 3), the scattering matrix is expressed as

$$S=P^{+}_{A\infty}O_A P_{CA}O_C P_{CTC}I_C P_{CA}I_A P^{-}_{A\infty} \ . \tag{2.16}$$

The matrix P_{XY} is diagonal and represents a propagation from point X to Y $(X<Y)$ without any transition. The matrix I_X (O_X) represents a nonadiabatic transition at the avoided crossing point X in the incoming (outgoing) segment of trajectory. These matrices are explicitly given by

$$[P^{+}_{A\infty}]_{nm}=[P^{-}_{A\infty}]_{nm}=\delta_{nm}\exp\left[i\int_A^{\infty}[k_n^K(R)-k_n^K(\infty)]dR - ik_n^K(\infty)A+\frac{i}{2}K\pi\right] , \tag{2.17}$$

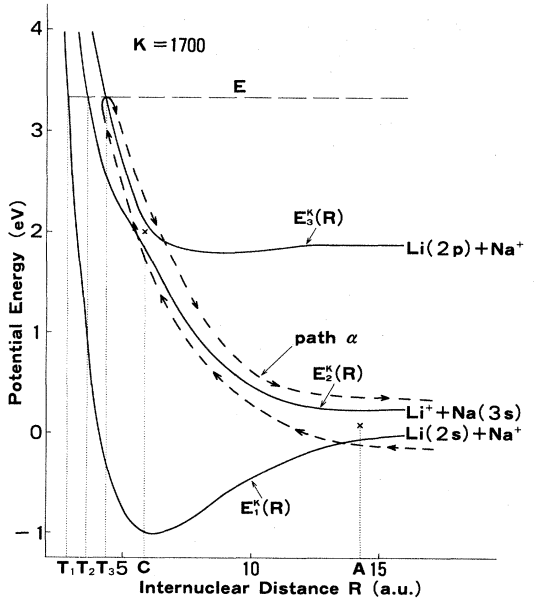

FIG. 3. Lowest three dynamical-state potential energy curves for $K=1700$. Dashed line is an example of possible paths for the transition $\mathrm{Li}(2s)+\mathrm{Na}^{+}\rightarrow\mathrm{Li}^{+}+\mathrm{Na}(3s)$.

$$[P_{XY}]_{nm}=\delta_{nm}\exp\left[i\int_X^Y k_n^K(R)dR\right] \quad (X<Y) , \tag{2.18}$$

$$[P_{XTX}]_{nm}=\delta_{nm}\exp\left[2i\int_{T_n}^X k_n^K(R)dR+i\pi/2\right] , \tag{2.19}$$

$$I_A=\begin{bmatrix}(1-p_{\mathrm{RZ}})^{1/2} & (p_{\mathrm{RZ}})^{1/2}\exp(i\sigma_A) & 0\\ -(p_{\mathrm{RZ}})^{1/2}\exp(-i\sigma_A) & (1-p_{\mathrm{RZ}})^{1/2} & 0\\ 0 & 0 & 1\end{bmatrix} , \tag{2.20}$$

$$I_C=\begin{bmatrix}1 & 0 & 0\\ 0 & (1-p_{\mathrm{LZ}})^{1/2}\exp(i\phi_S^C) & (p_{\mathrm{LZ}})^{1/2}\exp(i\sigma_C)\\ 0 & -(p_{\mathrm{LZ}})^{1/2}\exp(-i\sigma_C) & (1-p_{\mathrm{LZ}})^{1/2}\exp(-i\phi_S^C)\end{bmatrix} , \tag{2.21}$$

and

$$[O_X]_{nm}=[I_X]_{mn} \ , \tag{2.22}$$

where

$$k_n^K(R)=\left[\frac{2\mu}{\hbar^2}(E-E_n^K(R))\right]^{1/2} , \tag{2.23}$$

$$p_{\mathrm{RZ}}=[1+\exp(2\delta_{\mathrm{RZ}})]^{-1} , \tag{2.24}$$

$$\sigma_A+i\delta_{\mathrm{RZ}}=\int_A^{R_*^A}[k_1^K(R)-k_2^K(R)]dR , \tag{2.25}$$

$$E_1^K(R_*^A)=E_2^K(R_*^A) , \tag{2.26}$$

$$p_{\mathrm{LZ}}=\exp(-2\delta_{\mathrm{LZ}}) , \tag{2.27}$$

$$\sigma_C+i\delta_{\mathrm{LZ}}=\int_C^{R_*^C}[k_2^K(R)-k_3^K(R)]dR , \tag{2.28}$$

$$E_2^K(R_*^C)=E_3^K(R_*^C) , \tag{2.29}$$

$$\phi_S^C=(\delta_{\mathrm{LZ}}/\pi)\ln(\delta_{\mathrm{LZ}}/\pi)-\delta_{\mathrm{LZ}}/\pi+\pi/4 - \arg\Gamma(1+i\delta_{\mathrm{LZ}}/\pi) . \tag{2.30}$$

It should be noted that the transition between the dynamical states $E_2^K(R)$ and $E_3^K(R)$ is the Landau-Zener (LZ) type, and the one between $E_1^K(R)$ and $E_2^K(R)$ is the Rosen-Zener (RZ) type.

In the actual calculations the impact parameter ρ defined by

$$\rho=(K+\tfrac{1}{2})/k\equiv(K+\tfrac{1}{2})/(k_i k_f)^{1/2} \tag{2.31}$$

is employed instead of K for simplicity, where k_i (k_f) is the asymptotic initial (final) wave number. The total cross section for the transition $i\rightarrow f$ is calculated as usual by

$$\sigma_{if}=2\pi\int_0^{\infty}d\rho\rho\,|S_{if}(\rho)|^2 . \tag{2.32}$$

As is seen from Eqs. (2.16)–(2.22), the scattering matrix element S_{if} can be generally expressed as

$$S_{if}=\sum_{\alpha}[P_{if}^{\alpha}(\rho)]^{1/2}\exp[i\phi_{if}^{\alpha}(\rho)] , \tag{2.33}$$

where the suffix α distinguishes the possible paths which

enter along the potential $E_i^K(R)$ and exit along $E_f^K(R)$, and P_{if}^α and ϕ_{if}^α represent the overall transition probability and the total phase along the path α, respectively. In the case of the path α shown in Fig. 3, for instance, the overall probability and the total phase can be explicitly given by

$$P_{12}^\alpha = p_{\mathrm{RZ}}(1-p_{\mathrm{RZ}})(p_{\mathrm{LZ}})^2 \tag{2.34a}$$

and

$$\phi_{12}^\alpha = 2\int_{T_3}^{C} k_3^K(R)dR + 2\int_C^A k_2^K(R)dR + \int_A^\infty [k_1^K(R)-k_1^K(\infty)]dR - k_1^K(\infty)A + \int_A^\infty [k_2^K(R)-k_2^K(\infty)]dR$$
$$-k_2^K(\infty)A - \sigma_A - 2\sigma_C + (K+\tfrac{3}{2})\pi \,. \tag{2.34b}$$

It should be noted that when a turning point becomes larger than an avoided crossing point at large impact parameters, the phase integral over that interval becomes pure imaginary and is added to the corresponding exponent δ. For instance, when the turning points T_1 and T_2 both are larger than A, the exponent δ_{RZ} is given by

$$\delta_{\mathrm{RZ}} = \mathrm{Im}\int_A^{R_*^A} [k_1^K(R)-k_2^K(R)]dR + \int_A^{T_2} |k_2^K(R)|\,dR - \int_A^{T_1} |k_1^K(R)|\,dR \,. \tag{2.35}$$

Accuracy of the Rosen-Zener and Landau-Zener-Stueckelberg (LZS) formulas in the form given here has been well investigated for the transitions between two states of the same symmetry.[18] The accuracy of the LZS formula in the DS representation for the Σ-Π transition will be demonstrated in Sec. II D.

C. Uniform semiclassical theory for differential cross sections

Once the DS representation is employed, a semiclassical theory for the calculation of not only total, but also differential, cross sections can be formulated without any ambiguity. The rotational coupling effect can be incorporated naturally.

The scattering amplitude for the transition $n\to m$ can be generally given by

$$f_{nm}(\theta) = \frac{1}{2ik_n}\sum_K (2K+1)S_{nm}^K P_K(\cos\theta) \,, \tag{2.36}$$

where $P_K(X)$ is the Legendre polynomial, and θ ($\geq 0°$) is the scattering angle. By using Eq. (2.31) and the conventional approximation

$$P_K(\cos\theta) \simeq \left[\frac{2}{\pi(K+\frac{1}{2})\sin\theta}\right]^{1/2} \cos[(K+\tfrac{1}{2})\theta - \tfrac{1}{4}\pi] \,, \tag{2.37}$$

which is valid when $\sin\theta \gtrsim 1/K$, and the expression (2.33) for S_{nm}^K, we obtain

$$f_{nm}(\theta) \simeq \left[\frac{k_n^2}{2\pi k\sin\theta}\right]^{1/2} \sum_\alpha \int d\rho [\rho P_{nm}^\alpha(\rho)]^{1/2} \times [\exp(i\varphi_-) - \exp(i\varphi_+)] \,, \tag{2.38}$$

where

$$\varphi_\pm = \phi_{nm}^\alpha \pm (k\rho\theta + \pi/4) \,. \tag{2.39}$$

The phase stationary points are the solutions of

$$\Theta_{nm}^\alpha(\rho) = \mp\theta \,, \tag{2.40}$$

where Θ_{nm}^α is the deflection function defined by

$$\Theta_{nm}^\alpha = \frac{\partial\phi_{nm}^\alpha}{\partial\rho} \,. \tag{2.41}$$

The integral involving φ_- in Eq. (2.38) can be evaluated, to good accuracy, by the stationary phase approximation, yielding

$$f_{nm}^{(-)}\theta \simeq \sum_\alpha [\sigma_{\alpha,nm}^{(3)}(\theta)]^{1/2}\exp(i\beta_{\alpha,nm}^{(-)} - i\pi/2) \,, \tag{2.42}$$

where $\sigma_{\alpha,nm}^{(3)}(\theta)$ is the classical cross section defined by

$$\sigma_{\alpha,nm}^{(3)}(\theta) = \frac{\rho_3}{\sin[d\Theta_{nm}^\alpha/d\rho]_{\rho_3}} \,, \tag{2.43}$$

$$\beta_{\alpha,nm}^{(-)} = \phi_{nm}^\alpha(\rho_3) - k\rho_3\theta \,, \tag{2.44}$$

and ρ_3 is the phase stationary point corresponding to φ_- (see Fig. 4). Since there exist two phase stationary points ρ_1 and ρ_2 in the integral involving φ_+ in Eq. (2.38), this integral should be evaluated by the uniform semiclassical approximation.[19–21] Then we have

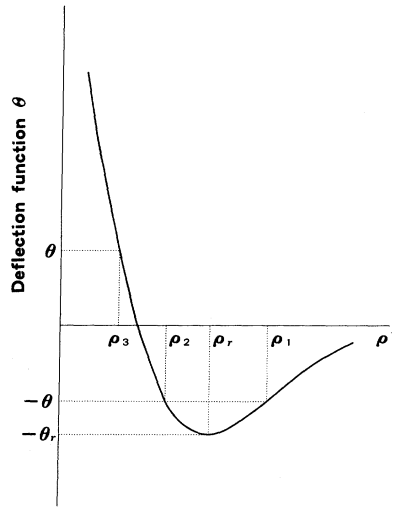

FIG. 4. Schematic diagram of deflection function Θ as a function of impact parameter ρ.

$$f_{nm}^{(+)}(\theta)\simeq\sum_{\alpha}\exp(i\beta_{\alpha,nm}^{(+)}+i5\pi/4)[A_{nm}^{\alpha}\mathrm{Ai}(-Z_{\alpha})+iB_{nm}^{\alpha}\mathrm{Ai}'(-Z_{\alpha})]\ , \tag{2.45}$$

where $\mathrm{Ai}(-Z)$ and $\mathrm{Ai}'(-Z)$ are the Airy function and its derivative,

$$A_{nm}^{\alpha}=\sqrt{\pi}Z_{\alpha}^{1/4}\{[\sigma_{\alpha,nm}^{(1)}(\theta)]^{1/2}+[\sigma_{\alpha,nm}^{(2)}(\theta)]^{1/2}\}\ , \tag{2.46}$$

$$B_{nm}^{\alpha}=\sqrt{\pi}Z_{\alpha}^{-1/4}\{[\sigma_{\alpha,nm}^{(1)}(\theta)]^{1/2}-[\sigma_{\alpha,nm}^{(2)}(\theta)]^{1/2}\}\ , \tag{2.47}$$

$$Z_{\alpha}=\{\tfrac{3}{4}[\phi_{nm}^{\alpha}(\rho_2)-\phi_{nm}^{\alpha}(\rho_1)+(\rho_2-\rho_1)\theta]\}^{2/3}\ , \tag{2.48}$$

and

$$\beta_{\alpha,nm}^{(+)}=\tfrac{1}{2}[\phi_{nm}^{\alpha}(\rho_2)+\phi_{nm}^{\alpha}(\rho_1)+(\rho_2+\rho_1)\theta]\ . \tag{2.49}$$

When $\theta\simeq\theta_r$ (rainbow angle) or $\theta\geq\theta_r$, we can conveniently use the following expressions instead of Eqs. (2.46)–(2.49):

$$A_{nm}^{\alpha}\simeq(12k)^{1/6}\left[\frac{\pi\rho_r}{\sin\theta}\right]^{1/2}\left[\frac{d^2\Theta_{nm}^{\alpha}}{d\rho^2}\right]_{\rho_r}^{-1/3}\ , \tag{2.50}$$

$$B_{nm}^{\alpha}\simeq\frac{1}{(12k)^{1/6}}\left[\frac{\pi}{\rho_r\sin\theta}\right]^{1/2}\left[\frac{d^2\Theta_{nm}^{\alpha}}{d\rho^2}\right]_{\rho_r}^{-2/3}\ , \tag{2.51}$$

$$Z_{\alpha}\simeq(\tfrac{3}{2}k)^{2/3}\left[\frac{d^2\Theta_{nm}^{\alpha}}{d\rho^2}\right]_{\rho_r}^{-1/3}(\theta-\theta_r)\ , \tag{2.52}$$

and

$$\beta_{\alpha,nm}^{(+)}\simeq\phi_{nm}^{\alpha}(\theta)+\rho_r\theta\ , \tag{2.53}$$

where ρ_r is the impact parameter corresponding to the rainbow angle. [We have found our Eqs. (2.50)–(2.53) to be slightly different from Eq. (11′) of Ref. 21.]

Thus, the differential cross sections can be calculated by

$$\sigma_{nm}(\theta)=|f_{nm}^{(-)}(\theta)+f_{nm}^{(+)}(\theta)|^2\ . \tag{2.54}$$

However, the experimentally observed differential cross sections are more often than not the low-resolution cross sections, which correspond to

$$\sigma_{nm}^{\mathrm{LR}}(\theta)=|f_{nm}^{(-)}(\theta)|^2+|f_{nm}^{(+)}(\theta)|^2\ . \tag{2.55}$$

We use this expression for a comparison with experiments. The cross sections calculated from Eqs. (2.54) oscillate rapidly with large amplitudes; thus are not very appropriate for the comparison with experiments. The period of this rapid oscillation is given by

$$\Delta\theta_r\simeq\frac{2\pi}{k|\rho_a+\rho_b|}\ , \tag{2.56a}$$

where ρ_a and ρ_b are the impact parameters corresponding to Θ and $-\Theta$, respectively.

On the other hand, the oscillation of $\sigma_{nm}^{\mathrm{LR}}(\theta)$ comes from the interference between the paths in the same branch ($\Theta>0$ or $\Theta<0$). The period of this oscillation is roughly equal to

$$\Delta\theta\simeq\frac{2\pi}{k|\rho_a-\rho_b|}\ , \tag{2.56b}$$

where ρ_a and ρ_b are the impact parameters corresponding to the same Θ.

D. Verification of the semiclassical theory for the Σ-Π transition in the two-state approximation

By taking 1Π and 2Σ adiabatic states we demonstrate here the applicability of the Landau-Zener-Stueckelberg formula in the DS representation to the study of the rotational coupling effect. The semiclassical results are compared with the quantum-mechanical close-coupling calculations. The LZS formula for transition probability is given by

$$P_{\mathrm{LZS}}=4p_{\mathrm{LZ}}(1-p_{\mathrm{LZ}})\sin^2\phi_{\mathrm{LZS}}\ , \tag{2.57}$$

where

$$\phi_{\mathrm{LZS}}=\sigma_C+\phi_S^C+\int_{T_2}^{C}k_2^K(R)dR-\int_{T_3}^{C}k_3^K(R)dR\ . \tag{2.58}$$

Transition probabilities are shown in Fig. 5 as a function of impact parameter. Since the step size of the impact parameter was not taken small enough in the case of 750 eV, the oscillations of transition probabilities at small ρ are not the exact reproduction of the real oscillations. How-

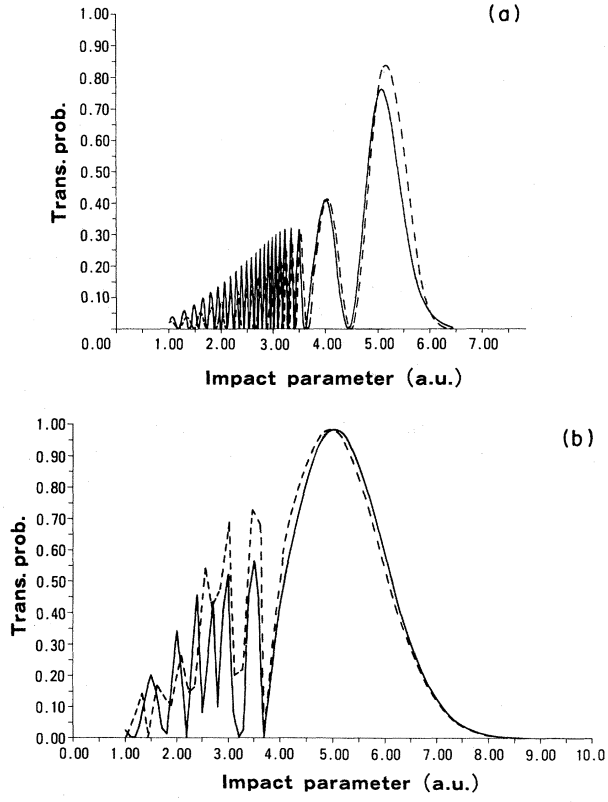

FIG. 5. Transition probabilities vs impact parameter for the transition $2\Sigma\rightarrow1\Pi$ (two-state approximation). Solid line: quantum-mechanical close-coupling calculation, and dashed line: present semiclassical theory. (a) $E_{\mathrm{rel}}=30$ eV and (b) $E_{\mathrm{rel}}=750$ eV.

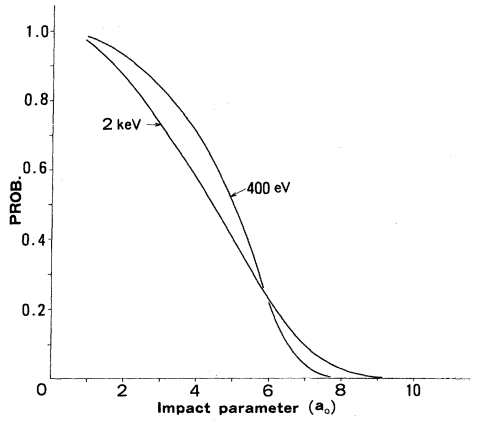

FIG. 6. Transition probabilities p_{LZ} for the one passage of the avoided crossing point as a function of ρ in the case of the 2Σ-1Π transition at $E_{rel}=400$ eV and 2 keV.

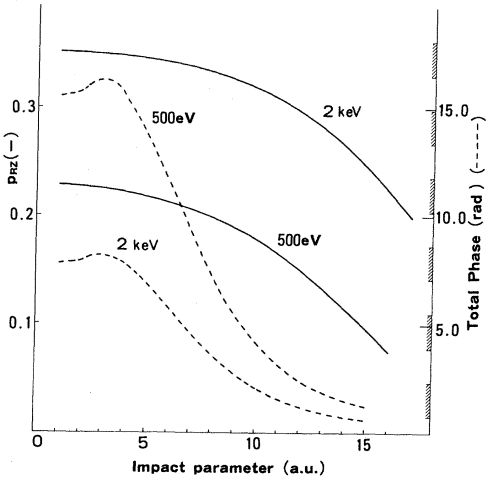

FIG. 8. Transition probabilities p_{RZ} (solid line) for the one passage of the pseudocrossing point and total phases (dashed line) as a function of impact parameter for the $1\Sigma\rightarrow 2\Sigma$ transition at $E_{rel}=500$ eV and 2 keV. The shaded regions correspond to $\sin^2(\text{total phase}) \geq \frac{1}{2}$.

ever, as is easily seen from these figures, the present analytic theory proves to be quite useful over a wide range of collision energy. Figure 6 shows the variation of the transition probability for one passage of the avoided crossing point against the impact parameter. This is compared with the corresponding one for the 1Σ-2Σ transition shown in Fig. 8.

III. TOTAL CROSS SECTIONS

A. Charge transfer: $Li(2s) + Na^+ \Longleftrightarrow Li^+ + Na(3s)$

Since our calculations were performed at energies relatively high compared to the asymptotic energy difference of 1Σ and 2Σ, the cross sections for the $1\Sigma\rightarrow 2\Sigma$ and $2\Sigma\rightarrow 1\Sigma$ transitions are almost equal to each other.

We have first carried out the two-state calculations. The results are shown in Figs. 7, 8, and 10 (see Fig. 9 also). The transition probabilities show an irregular oscillation as a function of ρ at small ρ This irregular oscillation causes an undulation of the total cross sections as a function of collision energy, as is seen in Fig. 10. This phenomenon has been discussed by several authors[6,22,23] and is due to the slow variation (appearance of optimum) of the total phase in the small-ρ region (see Fig. 8).

Despite the small energy difference ($\simeq$0.253 eV) between 1Σ and 2Σ at $R=\infty$, the transition is not the exact resonance type even at 2 KeV of collision energy. Figure 8 also shows the transition probability p_{RZ} as a function of impact parameter. The ρ dependence is weak compared to that of p_{LZ} shown in Fig. 6. An additional calculation was carried out by replacing the adiabatic-state energy $\epsilon_{2\Sigma}(R)$ by the dynamical-state energy $E_2(R)$ in order to see the effect of the rotational coupling on the transition between the two lowest states. Since the pseudocrossing point between 1Σ and 2Σ is located at large R, the rotational coupling hardly affects the radial coupling.

The results of the three-state calculations are shown in Figs. 9 and 10. The energy dependence (not the magnitude) of the cross sections are in fairly good accordance with those of Melius and Goddard. The calculated total cross sections are larger than those of Melius and Goddard. This is presumably due to the small discrepancy of the adiabatic potential energies at large R ($\gtrsim 12a_0$), since $\mathrm{Im}(R_*^A)$ (thus p_{RZ}) is sensitive to a small variation of the

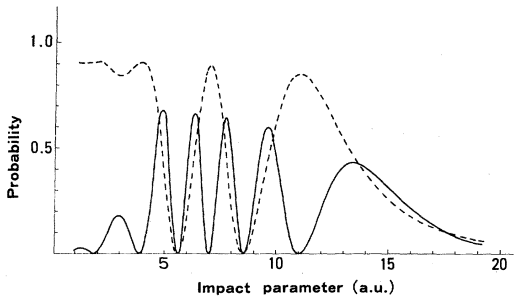

FIG. 7. Transition probabilities vs impact parameter for the $1\Sigma\rightarrow 2\Sigma$ transition (two-state approximation). Solid line: $E_{rel}=500$ eV, and dashed line: $E_{rel}=2$ keV.

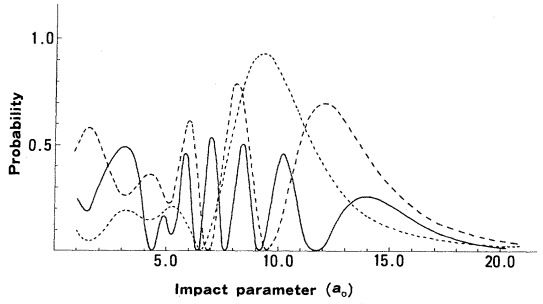

FIG. 9. Transition probabilities vs impact parameter for the 1Σ-2Σ transition (three-state calculation). Solid line: $E_{rel}=333$ eV. Dashed line: $E_{rel}=1$ keV. Dotted line: $E_{rel}=3.7$ keV.

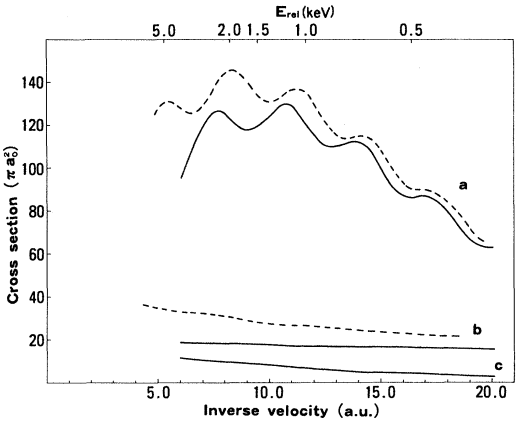

FIG. 10. Total cross sections as a function of inverse relative velocity. (a) $1\Sigma \rightarrow 2\Sigma$ transition, (b) $2\Sigma \rightarrow 1\Pi$ transition, and (c) $1\Sigma \rightarrow 1\Pi$ transition. Solid line: three-state ($1\Sigma, 2\Sigma, 1\Pi$) calculation. Dashed line: two-state calculation.

potentials in this region. Throughout this paper we use the potential energies given by Wijnaendts van Resandt *et al.*, since there are no other analytic expressions available. Usage of much more accurate adiabatic potential energies, therefore, would change the magnitudes of the cross sections, but would not affect largely the qualitative features of the cross sections.

B. Excitation to Li($2p$) + Na^+

Figure 11 shows the probabilities as a function of impact parameter for the transitions $1\Sigma \rightarrow 1\Pi$ and $2\Sigma \rightarrow 1\Pi$.

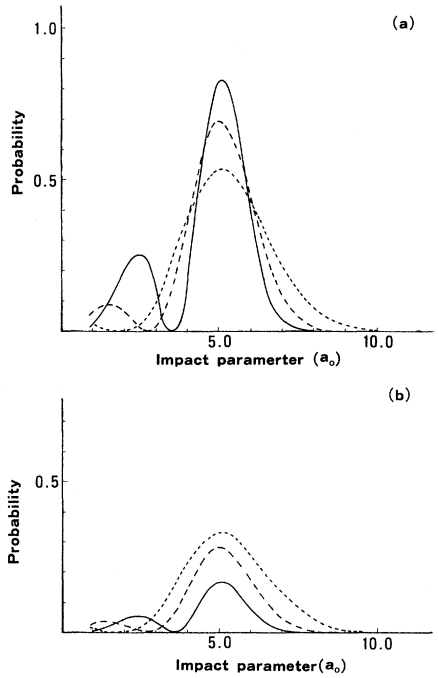

FIG. 11. Transition probabilities vs impact parameter (three-state calculation). (a) $2\Sigma \rightarrow 1\Pi$ transition and (b) $1\Sigma \rightarrow 1\Pi$ transition. Solid line: $E_{\rm rel} = 333$ eV. Dashed line: $E_{\rm rel} = 1$ keV. Dotted line: $E_{\rm rel} = 3.7$ keV.

As is easily understood by considering the possible paths for these transitions, the ratio of the transition probability for $2\Sigma \rightarrow 1\Pi$ to that for $1\Sigma \rightarrow 1\Pi$ is simply equal to $(1-p_{\rm RZ})/p_{\rm RZ}$. As is seen from Fig. 8, $p_{\rm RZ}$ varies slowly in the region of impact parameter where the rotationally induced transitions are appreciable. Therefore the transition probabilities for $2\Sigma \rightarrow 1\Pi$ and $1\Sigma \rightarrow 1\Pi$ have generally the same shape as a function of impact parameter. Since $p_{\rm RZ}$ is rather small at energies $\lesssim 1$ keV, the probability for $2\Sigma \rightarrow 1\Pi$ is larger than that for $1\Sigma \rightarrow 1\Pi$. This difference becomes, however, smaller with collision energy, since $p_{\rm RZ} \rightarrow 0.5$ when $E \rightarrow \infty$. The total cross sections are shown in Fig. 10. They are smaller than those of Melius and Goddard. The reason for this is basically the same as that mentioned above, namely the transition between 1Σ and 2Σ is more favorable than that in the case of Melius and Goddard.

IV. DIFFERENTIAL CROSS SECTIONS

In this section the calculated results of the low-resolution differential cross sections defined by Eq. (2.55) are reported and are compared with experiments. Basic quantities needed to evaluate the scattering amplitudes $f_{nm}^{(-)}(\theta)$ and $f_{nm}^{(+)}(\theta)$ given by Eqs. (2.42) and (2.45) are phases ϕ_{nm}^{α}, exponent parameters $\delta_{\rm LZ}$ and $\delta_{\rm RZ}$, and deflection functions Θ_{nm}^{α} defined by Eqs. (2.33), (2.25), (2.28), and (2.41), respectively. The deflection functions were computed by transforming the integral variable R to γ by $R = T\cos\gamma$, since the integrands diverge as $\sim(R-T)^{-1/2}$. [24] It should be noted that phases ϕ_{nm}^{α} include the contributions $\sigma_{A,C}$ from the complex integrals (2.25) and (2.28), and the Stokes phase ϕ_S^C defined by Eq. (2.30). In the calculations of $f_{nm}^{(+)}(\theta)$, expressions (2.46)—(2.49) were used at scattering angles smaller than the rainbow angle ($\theta < \theta_r$). At scattering angles very close to or larger than θ_r, expressions (2.50)—(2.53) were utilized. A spline fit was made to the numerical data of deflection functions. Their derivatives were calculated by using these spline functions. The scattering angle in the laboratory system (θ_L) is related to that in the center-of-mass system (θ) by

$$\tan\theta_L = \frac{\sin\theta}{m_p/m_t + \cos\theta} , \tag{4.1}$$

where m_p (m_t) is the mass of projectile (target) atom.

The differential cross sections presented in this section are the reduced cross sections defined as

$$Q(\theta) = \sigma^{\rm LR}(\theta)\,\theta\sin\theta . \tag{4.2}$$

Since the experimental data are relative, they are normalized to the corresponding theoretical results at peak values except for the $1\Sigma \rightarrow 2\Sigma$ transition at 2 keV (Fig. 15). The differential cross sections reported here are those at scattering angles less than several mrad, because the larger angle scattering is mainly determined by the potentials at small R which were estimated by the rather arbitrary extrapolation procedure mentioned before and could not be the real one.

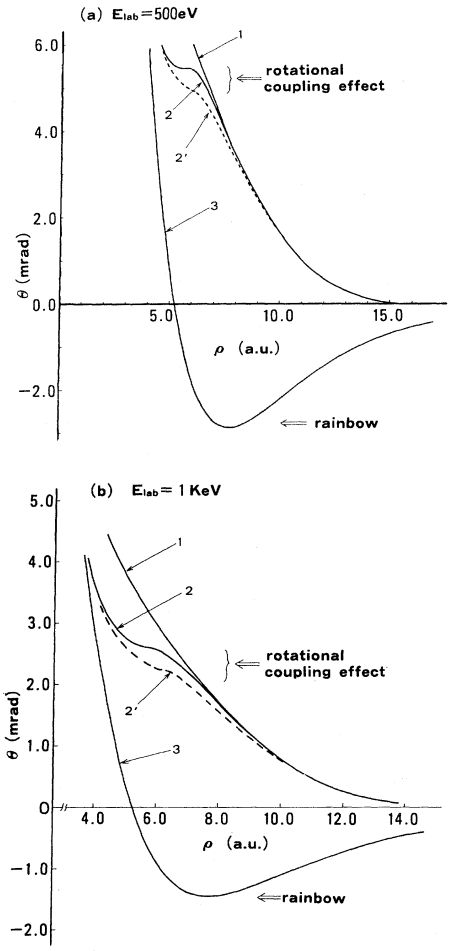

FIG. 12. Deflection functions for the $1\Sigma\rightarrow 2\Sigma$ transition. 1, path $1\rightarrow 2\rightarrow 3\rightarrow T_3\rightarrow 3\rightarrow 2$ $(1\Sigma\rightarrow 2\Sigma)$ and path $2\rightarrow 3\rightarrow T_3\rightarrow 3\rightarrow 2\rightarrow 1$ $(2\Sigma\rightarrow 1\Sigma)$; 2, path $1\rightarrow 2\rightarrow T_2\rightarrow 2$ $(1\Sigma\rightarrow 2\Sigma)$; 2′, path $2\rightarrow T_2\rightarrow 2\rightarrow 1$ $(2\Sigma-1\Sigma)$; 3, path $1\rightarrow T_1\rightarrow 1\rightarrow 2$ $(1\Sigma\rightarrow 2\Sigma)$ and path $2\rightarrow 1\rightarrow T_1\rightarrow 1$ $(2\Sigma\rightarrow 1\Sigma)$. The number j $(=1-3)$ indicates the jth dynamical state and T_j the turning point. (a) $E_{\rm lab}=500$ eV and (b) $E_{\rm lab}=1$ keV.

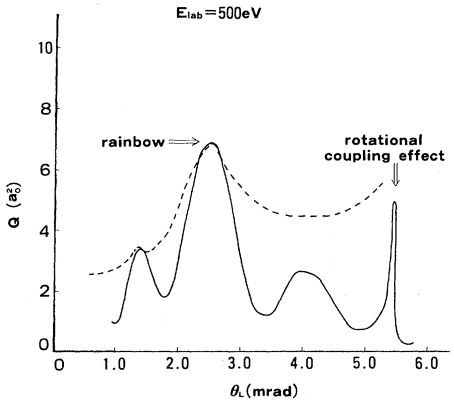

FIG. 13. Differential cross sections for the $1\Sigma\rightarrow 2\Sigma$ transition at $E_{\rm lab}=500$ eV. Solid line: present theory. Dashed line: experiment (Ref. 10).

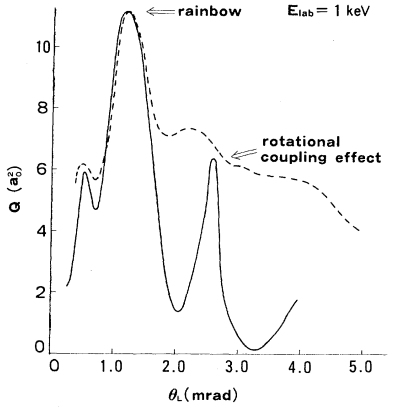

FIG. 14. Same as Fig. 13 at $E_{\rm lab}=1$ keV.

A. Charge transfer from $Na^+ + Li(2s)$ $(1\Sigma\rightarrow 2\Sigma)$

The deflection functions for this transition are shown in Fig. 12 for 500 eV and 1 keV. They are defined by Eq. (2.41) and can be calculated without any ambiguity. There are three possible paths. The path 1 corresponds to a trajectory $1\rightarrow 2\rightarrow 3\rightarrow T_3\rightarrow 3\rightarrow 2$, where the number j $(=1-3)$ indicates the jth dynamical state and T_j the turning point. The paths 2 and 3 correspond to $1\rightarrow 2\rightarrow T_2\rightarrow 2$ and $1\rightarrow T_1\rightarrow 1\rightarrow 2$, respectively. The rotational coupling effect is clearly manifested in the deflection function for path 2. The slope of the deflection function in the corresponding region of ρ becomes smaller as the collision energy decreases. This causes a very narrow sharp peak in the differential cross section at lower collision energies (see Fig. 13).

The calculated differential cross sections are shown in Figs. 13–16. They are generally in good agreement with experiments, including the low-frequency oscillations, although the data points of Okamoto *et al.* are not sufficient for a detailed comparison. The peaks due to the rotational coupling are more clearly manifested in the

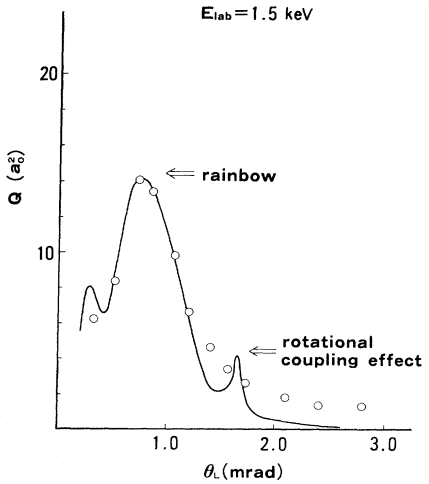

FIG. 15. Same as Fig. 13 at $E_{\rm lab}=1.5$ keV. Solid line: present theory. Open circle: experiment (Ref. 9).

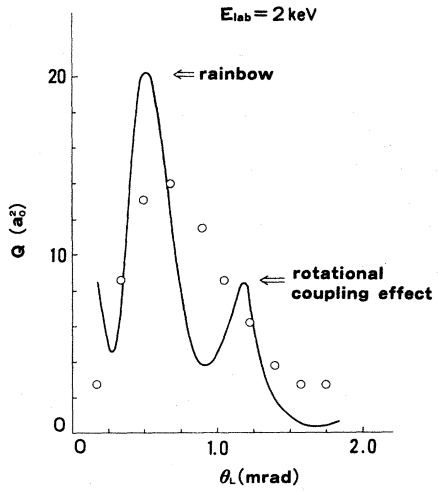

FIG. 16. Same as Fig. 15 at $E_{lab}=2$ keV.

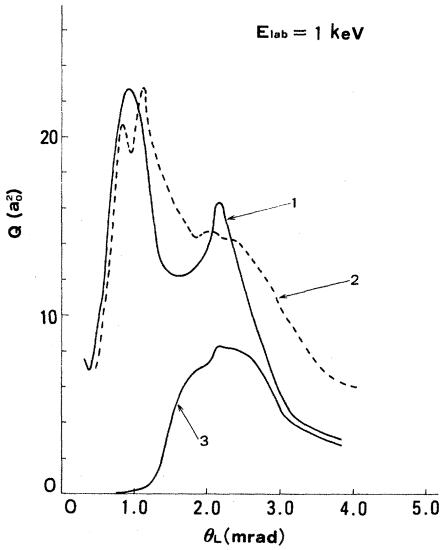

FIG. 18. Differential cross sections for the $2\Sigma\rightarrow 1\Pi$ transition and for the total charge transfer from $Li^+ + Na(3s)$ at $E_{lab}=1$ keV. 1, present theory (total charge transfer $2\Sigma\rightarrow 1\Sigma+1\Pi$). 2, experiment (total charge transfer) (Ref. 10). 3, present theory ($2\Sigma\rightarrow 1\Pi$ contribution).

theoretical results than in experiments. The rainbow peaks are also well reproduced by our semiclassical theory. The quasidiabatic potentials used by Wijnaendts van Resandt *et al.* are not necessary.

B. Charge transfer from $Li^+ + Na(3s)$ ($2\Sigma\rightarrow 1\Sigma,1\Pi$)

The deflection functions for the transition $2\Sigma\rightarrow 1\Pi$ are shown in Fig. 17. There are two possible paths. Path 1 is $2\rightarrow 3\rightarrow T_3\rightarrow 3$ and path 2 is $2\rightarrow T_2\rightarrow 2\rightarrow 3$. Figures 18–20 show the differential cross sections for the total charge transfer ($2\Sigma\rightarrow 1\Sigma+1\Pi$) and also the contributions of the transition $2\Sigma\rightarrow 1\Pi$. The general tendency is well reproduced by the theory, although the agreement between theory and experiment is not so good as in the $1\Sigma\rightarrow 2\Sigma$ case. In the experiments some of the high-frequency oscillations are observed, while the theoretical results shown are those only with low-frequency oscillations. The cross sections calculated from Eq. (2.54) oscillate rapidly with a period of $\sim$0.5 mrad. This oscillation is qualitatively in good accordance with experiments. A contribution of the $2\Sigma\rightarrow 1\Pi$ transition becomes dominant at larger angles. This is due to the fact that the rotationally induced transition takes place more effectively at smaller impact parameters compared to the Rosen-Zener–type transition between two Σ states (see the ρ dependence of p_{LZ} and p_{RZ} in Figs. 6 and 8). This contribution shifts to smaller angles as the collision energy increases.

Peaks in the theoretical results at $\theta_L\simeq 2.2$ mrad in the case of 1 keV and at $\theta_L\simeq 4.8$ mrad in the case of 500 eV represent the rotational coupling effects in the Σ-Σ transition (cf. Figs. 13 and 14). These peaks are not conspicuous in the experiments.

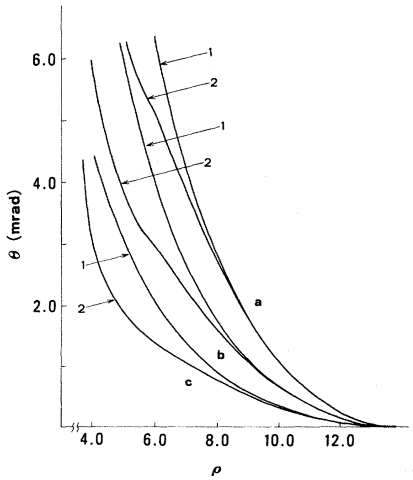

FIG. 17. Deflection functions for the $2\Sigma\rightarrow 1\Pi$ transition. 1, path $2\rightarrow 3\rightarrow T_3\rightarrow 3$; 2, path $2\rightarrow T_2\rightarrow 2\rightarrow 3$. (a) $E_{lab}=300$ eV, (b) $E_{lab}=500$ eV, and (c) $E_{lab}=1$ keV.

V. CONCLUDING REMARKS

The semiclassical theory based on the DS representation presented in this paper was proved to be an effective

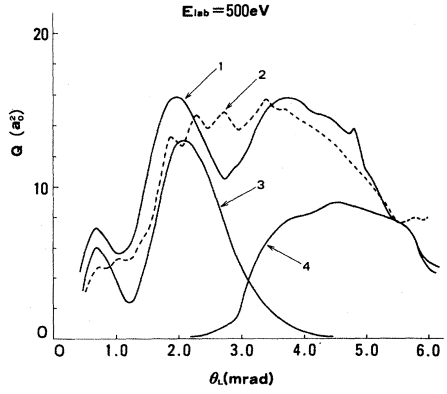

FIG. 19. Same as Fig. 18 at $E_{lab}=500$ eV. 3, present theory (rainbow contribution). 4, present theory ($2\Sigma\rightarrow 1\Pi$ contribution).

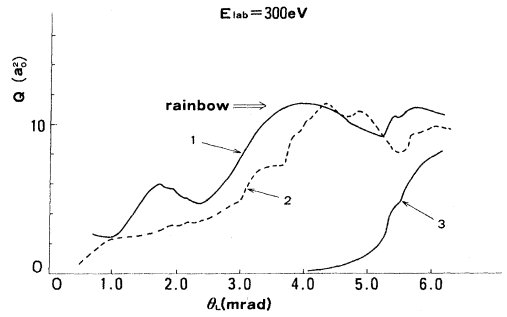

FIG. 20. Same as Fig. 18 at $E_{\text{lab}}=300$ eV.

unambiguous method to calculate differential as well as total cross sections for the collision processes involving both radial and rotational couplings. Understanding the mechanism of rotationally induced transitions can be cast into the same level as that of the ordinary radially induced transitions once we employ the DS representation. That is to say, by looking at the potential curves of the *dynamical* states we can understand the mechanisms of collision processes in terms of the conventional idea of the Landau-Zener (or the Rosen-Zener) transitions. The DS representation enables us to incorporate the multitrajectory effect naturally, and thus to uniquely define the deflection functions for any transitions. This makes an interpretation of the differential cross sections easier. One difficulty of the theory is the necessity of analytic continuation of potential energies into the complex R plane. It should be noted, however, that the full forms of the LZS and RZ formulas given here are quite accurate and that their simplifications would occassionally lead to errors.[18,25]

The calculated results on the $(\text{LiNa})^+$ collisions are in fairly good agreement with experiments. The absolute values of the calculated cross sections, however, would not be very reliable. This is attributed to the accuracy of the adiabatic potential energy curves, especially to the accuracy of the potential energies of the 1Σ and 2Σ states at large R (in the region of pseudocrossing). The transition probability p_{RZ} is directly dependent on the imaginary part of the complex zero of the energy difference between 1Σ and 2Σ; and the position of the zero is very sensitive to a slight variation of the potential energy curves in that region of R. Thus the magnitude of the Σ-Σ transition is most sensitive to this variation of the potentials. Other features reported in this paper would not be largely affected by this variation.

The other possible factor which would affect the Σ-Σ transition is an effect of the so-called electron translation factor (ETF). The ETF effect on the RZ-type transition would not probably be negligible, although this problem has not yet been fully investigated. The ETF's lead to an additional coupling term.[26] As in the case of the DS representation, we can define new basis states by diagonalizing the Hamiltonian matrix composed not only of the matrix of H_{dyn}, but also of this new coupling matrix (matrix A of Ref. 26). Then, exactly the same formulation as the one presented in this paper, but based on this new representation, would give a more complete semiclassical theory with even the ETF effects incorporated.

ACKNOWLEDGMENT

Numerical calculations have been carried out at the computer center of the Institute for Molecular Science.

*Present address: Institute of Applied Physics, University of Tsukuba, Sakura, Ibaraki 305, Japan.

[1](a) H. Nakamura and M. Namiki, J. Phys. Soc. Jpn. 49, L843 (1980); (b) Phys. Rev. A 24, 2963 (1981); 28, 486 (1983).

[2]H. Nakamura, Phys. Rev. A 26, 3125 (1982); 28, 486 (1983).

[3]Vo Ky Lan, M. LeDournouf, and J. M. Launay, in *Electron-Atom and Electron-Molecule Collisions,* edited by J. Hinze (Plenum, New York, 1982), p. 161.

[4]U. Fano, Phys. Rev. A 24, 2402 (1981); Rep. Prog. Phys. 46, 97 (1983).

[5]H. Nakamura, in *Invited papers of the Thirteenth International Conference on the Physics of Electronic and Atomic Collisions, Berlin, 1983,* edited by J. Eichler *et al.* (North-Holland, Amsterdam, 1984); (b) J. Phys. Chem. (special issue for 8th Canadian Symposium on Theoretical Chemistry, 1983) (in press).

[6]C. F. Melius and W. A. Goddard III, Phys. Rev. A 10, 1541 (1974).

[7](a) F. von Busch, J. Hormes, and H. D. Liesen, Chem. Phys. Lett. 34, 244 (1975); (b) *ibid.* 35, 372 (1975).

[8]P. Habitz and W. H. E. Schwarz, Chem. Phys. Lett. 34, 248 (1975).

[9](a) R. W. Wijnaendts van Resandt, R. L. Champion, and J. Los, Chem. Phys. 20, 107 (1977); (b) *ibid.* 26, 223 (1977).

[10]R. W. Wijnaendts van Resandt, C. de Vreugd, R. L. Champion, and J. Los, Chem. Phys. 29, 151 (1978).

[11]J. Grosser, Chem. Phys. 30, 187 (1978).

[12]T. Okamoto, Y. Sato, N. Shimakura, and Inouye, J. Phys. B 14, 2379 (1981).

[13]B. Hird and S. P. Ali, Can. J. Phys. 59, 576 (1981).

[14]F. von Busch, J. Hormes, and D. Liesen, J. Phys. B 15, 3695 (1982).

[15]F. von Busch, J. Phys. B 15, 3707 (1982).

[16]A. E. Orel and K. C. Kulander, J. Chem. Phys. 79, 1326 (1983).

[17]See, for instance, M. S. Child, *Molecular Collision Theory* (Academic, London, 1974).

[18]A. Barany and D. S. F. Crothers, Phys. Scr. 23, 1096 (1981).

[19]C. Chester, B. Friedman, and F. Ursell, Proc. Cambridge Philos. Soc. 53, 599 (1957).

[20]M. V. Berry, Proc. Phys. Soc. London 89, 479 (1966).

[21]J. M. Mullen and B. S. Thomas, J. Chem. Phys. 58, 5216 (1973).

[22]F. J. Smith, Phys. Lett. 20, 271 (1966).

[23]J. Perel, Phys. Rev. A 1, 369 (1970).

[24]G. E. Ioup and B. S. Thomas, J. Chem. Phys. 50, 5009 (1969).

[25]D. S. F. Crothers, Adv. At. Mol. Phys. 17, 55 (1981).

[26]M. Kimura and W. R. Thorson, Phys. Rev. A 24, 1780 (1981).